Scattering by a two-dimensional doped photonic crystal presenting an optical Kerr-effect

Pierre Godard, Frédéric Zolla, André Nicolet

SCATTERING BY A 2-DIMENSIONAL DOPED PHOTONIC CRYSTAL PRESENTING AN OPTICAL KERR EFFECT

Pierre Godard, Frédéric Zolla, André Nicolet

Abstract

Purpose We are interested in the two dimensional electromagnetic diffraction by a finite set of parallel non-linear rods (optical Kerr effect). In order to point out the versatility of our approach, a nonlinear (Kerr-effect) finite crystal is considered.

Design / methodology / approach We use a method christened "method of the virtual antenna" which allows to simulate an electromagnetic wave radiated by distant sources by the same electromagnetic wave radiated by nearby fictitious sources. This latest problem is then solved by a finite element method.

Findings The transmission through a finite Kerr crystal doped by a microcavity is given and a resonant wavelength is obtained. We then show that, at this resonant wavelength, the nonlinearity has a large influence on the local electromagnetic wave.

Originality / value We check the results via a verification of the power balance.

Keywords Nonlinear electromagnetic, Kerr-effect, scattering, photonic crystal, power balance, finite element method.

Paper type Research paper.

1 Introduction

We study the scattering by a non-linear finite photonic crystal, made of rods that are invariant along one direction, taken as the z-axis. The non-linearity is an optical Kerr effect (see, for example, [1]). For the time being, we restrict ourselves to an isotropic $\chi^{(3)}$ medium, so that we are concerned only with the $(\varepsilon_r)_{zz}$ component (indices are dropped from now on). Thus, in the crystal, $\varepsilon_r(\mathbf{E}) := \varepsilon_r^{(1)} + \chi^{(3)}|\mathbf{E}|^2$, where $\mathbf{E}$ is the (total) electric field. The rods are homogeneous, in the sense that $\varepsilon_r^{(1)}$ and $\chi^{(3)}$ are constant scalar fields: $\chi^{(3)}$ will be restricted to $\mathbb{R}$, and $\varepsilon_r^{(1)}$ will be real or complex, respectively when a lossless or lossy medium will be considered.

The crystal, considered as nonmagnetic, is surrounded by a vacuum. Because of the form of the optical Kerr effect, there is no harmonic generation. Hence it is meaningful to treat the electromagnetic field as a monochromatic field. Moreover, for the sake of simplicity only TM fields are tackled. A function $u : \mathbb{R}^2 \to \mathbb{C}$ can thus be defined such that $\mathbf{E}(x, y, z, t) = \Re e\{u(x, y)e^{i\omega t}\}\hat{z}$, and hence the non-linear equation to solve is

$$\Big(\triangle + k_0^2 \varepsilon_r(u)\Big) u = \mathfrak{s}, \tag{1}$$

with $u := u^s + u^i$, where u^s is the unknown scattered field satisfying an outgoing wave condition (OWC), and u^i is a given incident field that satisfies

$$\Big(\triangle + k_0^2\Big) u^i = \mathfrak{s}.$$

The source $\mathfrak{s}$ of u^i can be currents, or it vanishes in the case of incident plane waves.

We handle this study by numerical simulation. The finite element method (FEM) revealed to be appropriate, for its ability to treat inhomogeneous permittivities (hence this method seems more accurate than [2] or [3]). We used the *Comsol Multiphysics* software, in which the non-linearity is treated by an iterative scheme (damped Newton method).

The OWC is taken into account through perfectly matched layers (PML) surrounding the region of physical interest, as described in [4].

2 Implementing the incident field: use of virtual antennas

When using methods like FEM, we have to put the source $\mathfrak{s}$ in the meshed area. This can be very inconvenient: if the charges and currents are far from the scattering objects, precision decreases or a higher data storage has to be allowed because a large domain has to be considered. Besides, when dealing with plane waves (or plane waves packet), we have to find a way to implement this incident field.

2.0.1 A first approach

A usual method to get round these difficulties is to work with the scattered field, namely u^s. In this way, the sources of the problem are automatically conveyed in the meshed area (under the condition, of course, that all obstacles are contained in the meshed area).

Let us develop this method in the linear case: subtracting

$$(\triangle + k_0^2) u^i = \mathfrak{s} \tag{2}$$

to

$$(\triangle + k_0^2 \varepsilon_r) u = \mathfrak{s},$$

we obtain the equation for the scattered field:

$$(\triangle + k_0^2 \varepsilon_r) u^s = k_0^2 (1 - \varepsilon_r) u^i.$$

The point is that $1 - \varepsilon_r$ vanishes outside the scattering object, and thus the source is the scattering medium (and hence it is in the meshed area).

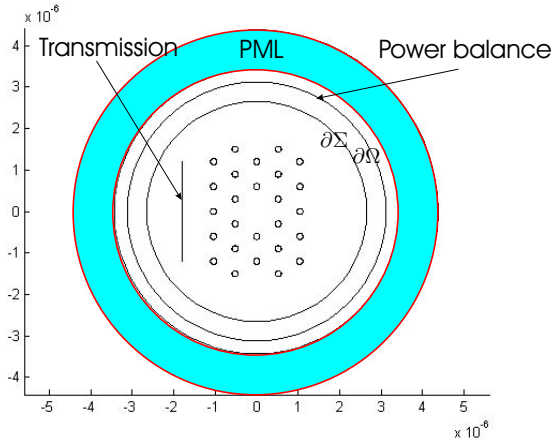

Figure 1: A cross-section of the studied system. The photonic crystal consists of twenty-six rods (the small circles on the image) invariant along one direction. The segment on left-hand side is used for extrapolation of the transmission coefficient. The four circles centered on the origin are, from the smallest to the largest: 1. $\partial\Sigma$, used for energy extrapolation, 2. $\Gamma := \partial\Omega$ on which the current of the virtual antenna flows, 3. the inner boundary of the PML, 4. the outer boundary of the PML.

Now, what happens in a medium, located in Ω_0, presenting an optical Kerr effect? Let us note Ξ_{Ω_0} the characteristic function of the set Ω_0, i.e., for a given point P in $\mathbb{R}^2$,

$$\Xi_{\Omega_0}(P) = \begin{cases} 1, & P \in \Omega_0 \\ 0, & \text{otherwise.} \end{cases}$$

The equation for the incident field is still (2), but the equation in Ω_0 for the total field is

$$\triangle u + k_0^2(\varepsilon_r^{(1)} + \chi^{(3)}|u|^2)u = 0.$$

The scattered field then satisfies

$$\triangle u^s + k_0^2(T_s(u^i, u^s)u^s + T_i(u^i, u^s)u^i) = k_0^2(1 - \varepsilon_r)u^i, \tag{3}$$

where

$$\begin{cases} \varepsilon_r := 1 + (\varepsilon_r^{(1)} - 1)\Xi_{\Omega_0} \\ T_s(u^i, u^s) := 1 + (\varepsilon_r^{(1)} + \chi^{(3)}|u^i + u^s|^2 - 1)\Xi_{\Omega_0} \\ T_i(u^i, u^s) := \chi^{(3)}|u^i + u^s|^2\Xi_{\Omega_0}. \end{cases}$$

We see that this propagation equation is far more difficult than the equation governing the total field; we thus decided to tackle the problem in a new route. For this purpose, a question arises: is it possible to simulate "any" sources $\mathfrak{s}$ by a source $\mathfrak{s}'$ close

to the scattering medium, such that the incident field, seen by the crystal, is the same? If the answer is "yes", then we could solve the problem for the total field.

2.0.2 Virtual antennas: from the principles to the implementation

The answer being yes, we give the principle in this subsection[1]: the incident field u^i is brought by a current $\mathbf{j} = \jmath\hat{z}$ located on a simple curve Γ (the interior of which is denoted by Ω - the scattering medium is strictly included in Ω) in the meshed area. More precisely, we find $\jmath$ such that it radiates a field u_v^i satisfying an OWC,

$$(\triangle + k_0^2)u_v^i = a\jmath\delta_\Gamma,$$

with a, a normalization constant, being equal to $i\omega\mu_0$, and such that u_v^i has the following fundamental property

$$u_v^i|_\Omega = u^i|_\Omega. \tag{4}$$

Because of 4, and the fact that the scattered medium is encompassed by Γ (i.e. $\Omega_0 \subset \Omega$), the equation for the scattered field, when restricted to Ω, is still (3). Consequently, the total field u in Ω does not depend on the way in which the incident field is implemented.

We called this process a *virtual antenna*. It is able to simulate almost any[2] incident field in a bounded region. It is worth noting that, out of Ω, u_v^i differs from u^i.

3 Acceptor modes in Kerr effect media

A particular simulation is now more detailed. We present a picture (figure 1) of a cross-section of the system under study.The incident field is a plane wave coming from the right ($u^i(x, y) = Ae^{ikx}$).

3.1 The acceptor mode

3.1.1 The transmission

A defect is created at the center of the crystal by removing one rod in order to obtain an "acceptor mode" ([2], [5], etc.); we show in the figure 2 the transmission (that is, the ratio of the energy flowing through the left segment when there is or when there is not the crystal) of the system. We note that it can be larger than one. Unless otherwise noted, the linear part of the relative permittivity is $\varepsilon_r^{(1)} = 8.41$ and the amplitude of the incident plane wave is $A = 1\,V/m$. We work with a wavelength in which the diameter of the rods is unity with an arbitrary unit (μm, for instance, in near infrared domain). We thus have $\lambda_r := \frac{\lambda}{d}$, d being the diameter of the rods.

[1] The reader will find in the appendix a rigorous formulation, the method to obtain the expression of **j** (see below) and a detailed computation for simulating, for example, a plane wave.

[2] we use here the terms "almost any" because, as it will be shown hereafter, for computing $\jmath$, we use a decomposition of u^i in a Fourier-Bessel series; since plane waves and waves generated by threads satisfy this condition, we consider that any physically canonical field can be simulated.

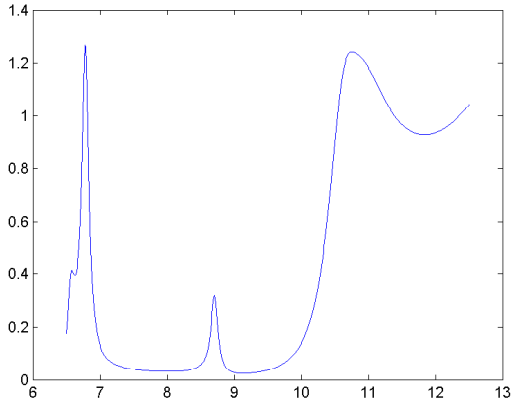

Figure 2: The transmission with respect to the relative wavelength $\lambda_r := \lambda/d$. A band gap ($\lambda_r \in [7, 10]$) and an acceptor mode ($\lambda_r \simeq 8.7$) can be noted.

The crystal behaves as a filter for $\lambda \in [7, 10]$, except for λ very close to 8.7: this wavelength is called the wavelength of the acceptor mode[3]. The wavelength of resonance being large compared to the dimension of the rods, the permittivity inside them is usually considered to be homogeneous [2]. This approximation is unnecessary with our method.

3.1.2 Maps of the fields

The real part of the electric fields in the linear and non-linear cases are reproduced in the figure 3. First we consider the acceptor mode. On the first image, 3(a), we are in the linear regime. We observe that the field in the microcavity can be as high as $5\,V/m$ (to be compared with the amplitude of the incident field: $A = 1\,V/m$). If the medium is nonlinear, this localization of the field can be enhanced (figure 3(b)) or lessened (figure 3(c)) according to the sign of the nonlinear coefficient.

The essential feature of the acceptor mode is to appear only at the resonant frequency - compare 3(a) with 3(d): there is no peak of the field in the microcavity if the wavelength is in the band gap. Hence, in the band gap, the variation of the field are too low for the nonlinearity to have an important effect.

Since the electric field u is inhomogeneous, and since the relative permittivity depends on it, the variation of the relative permittivity is also inhomogeneous. It is represented on the figure 4. The innermost rods have a change of relative permittivity as high as[4] $\frac{0.14}{8.41} = 1.7\%$; on the other hand, the electric field far from the microcavity is

[3] to fix the ideas about the dimensions, the pitch of the crystal is $\Lambda/d = 4$, and so the radius r_d of the defect is around $r_d \simeq 8\,d$.

[4] we note that, contrary to [3], the variation in each rod is not cylindrically symmetric. Moreover, 1.7% being higher that one encounters in experiment, the convergence of the programs is not limited by the value

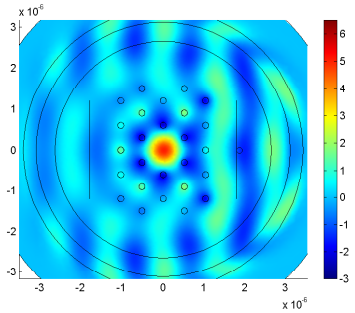

(a) $\chi^{(3)} = 0\, V^2/m^2$, $\lambda_r = 8.7$.

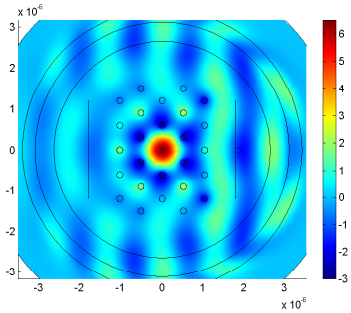

(b) $\chi^{(3)} = -10^{-2}\, V^2/m^2$, $\lambda_r = 8.7$.

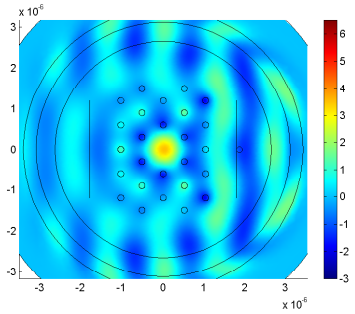

(c) $\chi^{(3)} = 10^{-2}\, V^2/m^2$, $\lambda_r = 8.7$.

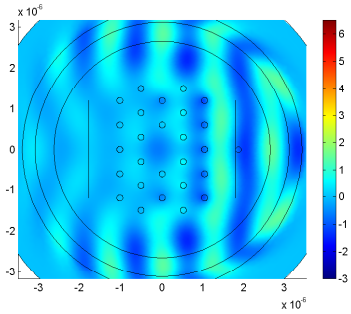

(d) $\chi^{(3)} = 0\, V^2/m^2$, $\lambda_r = 8.3$.

Figure 3: The real part of the total electric field $\Re e\{u\}$, in V/m, for different values of $\chi^{(3)}$ (zero in 3(a) and 3(d), negative in 3(b) and positive in 3(c)) and different wavelengths (the resonant wavelength $\lambda_r = \lambda_a$ in 3(a), 3(b) and 3(c), and in the gap in 3(d)).

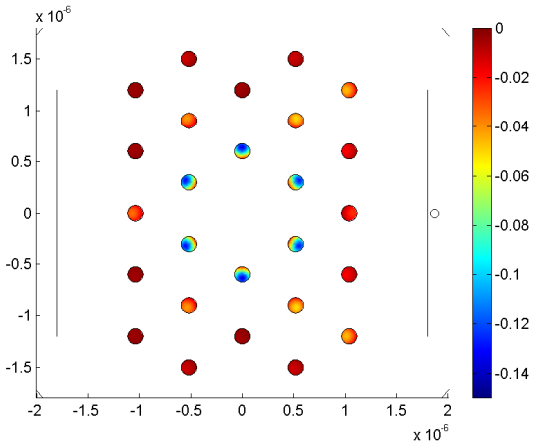

Figure 4: The variation of the relative permittivity, $\chi^{(3)}|u|^2 = \varepsilon_r - \varepsilon_r^{(1)}$, with $\lambda_r = \lambda_a$ and $\chi^{(3)} = -10^{-2}\, V^2/m^2$.

too small to significantly affect the relative permittivity of the outermost rods. In [2] or [5], the case in which only the central rods are nonlinear is studied.

3.1.3 The differential cross-section

We are concerned in this section in the direction in which the fields escape from the crystal.

The circle $\partial\Sigma$ (cf fig.1) completely encompasses the crystals. Hence, on that curve, the scattered field, which satisfies the Helmholtz equation, can be expanded in the Fourier-Bessel basis[5]:

$$u^s|_{\partial\Sigma}(r,\theta) = \sum_{n\in\mathbb{Z}} b_n H_n^{(2)}(kr) e^{in\theta}|_{r=r_0},$$

where k is the wave vector in free space and r_0 is the radius of $\partial\Sigma$. Since

$$H_n^{(2)}(z) \sim_{z\to\infty} \sqrt{\frac{2}{\pi z}} e^{i(-z+n\pi/2+\pi/4)} + o(1),$$

the following map is bounded and *a priori* nonzero for an incident plane wave:

$$\sigma(\theta) = \lim_{r\to\infty} 2\pi r \frac{|\mathbf{E}^s(r,\theta)|^2}{|\mathbf{E}^i(r,\theta)|^2}.$$

of the nonlinear parameter $\chi^{(3)}$.

[5]the development is in the $H_n^{(2)}$ functions because of our convention about the Fourier transform and the outgoing wave condition.

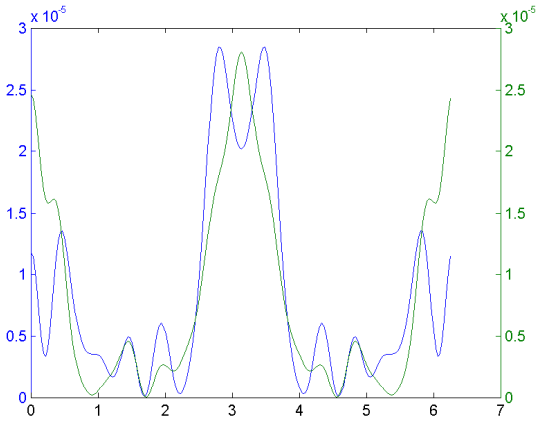

Figure 5: The differential cross section σ; blue: $\lambda_r = 8.7$ (the resonant wavelength), green: $\lambda_r = 8.3$ (in the gap).

This is the definition of the differential cross section (DCS). As seen in the figure 3, outside the microcavity, the nonlinearity has nearly no effect on the fields, and hence it has nearly no effect on the DCS.

The DCS is presented in the figure 5 for two wavelengths, the one of resonance and one in the band gap. We note that, for small changes in the frequency, the directions of radiation completely differ, especially for the backward ($\theta \simeq 0$) and the forward scattering ($\theta \simeq \pi$).

3.2 Power balance

In order to check the model coherence and the precision of the used numerical algorithms, we study the dissipated power. We choose the parameters as follows: the linear relative permittivity is $\varepsilon_r^{(1)} = 8.41 - 2i$ and the non-linearity coefficient is $\chi^{(3)} = -10^{-2}\, m^2/V^2$. Let Σ be the innermost disk of figure 1 with origin as center. Since its boundary is in the vacuum area, the (line density of the average over a time period of the) electromagnetic power $\mathcal{P}_e^{harm}$ flowing through Σ can be easily derived:

$$\int_\Sigma \mathcal{P}_e^{harm}\, ds = -\int_{\partial\Sigma} \Re(\hat{\mathbf{P}}) \cdot \hat{\mathbf{n}}\, dl,$$

$\Re(\hat{\mathbf{P}})$ being the real part of the complex Poynting vector, $\partial\Sigma$ the boundary of Σ, and $\hat{\mathbf{n}}$ the unit normal vector.

Denoting by ε_r'' the imaginary part of the relative permittivity, one also has[6]

[6] we obtain one expression from the other by the use of the propagation equation (1) satisfied by u and an application of Stoke's theorem.

$$\int_\Sigma \mathcal{P}_e^{harm}\, ds = -\frac{\varepsilon_0 \omega}{2} \int_\Sigma \varepsilon_r"(u)|u|^2\, ds.$$

This expression is the electromagnetic power lost inside Σ, i.e. in the crystal.

The comparison of the two expressions for $\int_\Sigma \mathcal{P}_e^{harm}\, ds$ gives a relative error of 8×10^{-5}, for linear and for non-linear crystals as well. From a numerical point of view, this is highly acceptable in view of the fact that one expression integrates $u\nabla\bar{u}$ on a line and the other one integrates $\varepsilon_r(u)|u|^2$ on a surface.

4 Conclusion

The scattering of electromagnetic waves on a medium presenting a nonnegligible optical Kerr-effect has been numerically studied in this article. The finite element method has been used, and this allows to avoid the usual approximation of the homogeneity of the relative permittivity in the rods. For the implementation of the incident field u^i, we use a method which substitutes u^i generated by a source S (possibly far from the scattered medium) by a field u_v^i generated by a current **j** flowing through a curve Γ located inside the meshed area. With this method, called the virtual antenna, almost any incident field can be simulated with a fictitious source at finite distance.

To confirm our simulation, a power balance has been checked. Moreover, the reaction of the crystal to an incident plane wave has been reported, through the transmission of the system, several maps of the electric field and the differential cross section.

Some of the technological applications of Kerr crystals are given, for example, in [6].

We give here the details about the computation of the current $\mathbf{j} = \jmath\hat{z}$ of the virtual antenna. We note u_v^i the field generated by $\mathbf{j}$ and u^i the incident field we intend to simulate. The relative permittivity of the host medium is ε_r; k_r is defined, as usually, by $k_r := k_0\sqrt{\varepsilon_r\mu_r} = k_0\sqrt{\varepsilon_r}$. Since we are dealing with the incident field, ε_r and k_r are just (possibly complex) numbers. Ω is a closed and simply-connected region of the plane, whose boundary $\Gamma := \partial\Omega$ is differentiable (we will use the normal vector along it).

The aim is to find a function $\jmath : \mathbb{R}^2 \to \mathbb{C}$ such that[7]

$$\Big(\triangle + k_r^2\Big)u_v^i = i\omega\mu_0\jmath\delta_\Gamma, \tag{5}$$

$$\lim_{r\to\infty} |\sqrt{r}\, u_v^i| < \infty, \quad \lim_{r\to\infty} \sqrt{r}(\frac{du_v^i}{dr} - ik_r u_v^i) = 0, \text{ [8]} \tag{6}$$

$$u_v^i|_{\dot\Omega} = u^i|_{\dot\Omega}. \tag{7}$$

We assume that u^i is unique[9] and satisfies

$$\Big(\triangle + k_r^2\Big)u^i = \mathfrak{s}, \tag{8}$$

$$|u^i(P)| < \infty \qquad \forall P \in \Omega. \tag{9}$$

The method is the following one: first consider that Ω is an infinitely conducting metal, illuminated by a source S; then

$$\Big(\triangle + k_r^2\Big)u = \mathfrak{s}, \qquad \text{in } \mathbb{R}^2\backslash\Omega \tag{10}$$

and u satisfies a Dirichlet condition on $\partial\Omega$. Besides, in Ω, the total field vanishes; hence, since S is obviously out of Ω, and so $Supp\{\mathfrak{s}\} \subset \mathbb{R}^2\backslash\Omega$, one also has

$$\Big(\triangle + k_r^2\Big)u = \mathfrak{s}, \qquad \text{in } \dot\Omega. \tag{11}$$

From the two last equations, we deduce:

$$\Big(\triangle + k_r^2\Big)u = \mathfrak{s} + [\frac{du}{dn}]\Big|_\Gamma \delta_\Gamma, \qquad \text{in } \mathbb{R}^2 \tag{12}$$

where, and from now on, u is a distribution.

The scattered field, $u^s := u - u^i$, thus satisfies the following equation, obtained by subtracting (12) by (8):

[7] Ω is a closed region, thus $\dot\Omega := \Omega\backslash\partial\Omega$.

[8] these two conditions are often summed up as the outgoing wave condition (OWC).

[9] we thus have to add a condition; in practice, this could be an OWC if we want to simulate a wave generated by a thread oriented along the z-axis, which encounters the plane we are considering in $\mathbf{r_0}$ and on which a current of intensity I flows; in that case $\mathfrak{s} = i\omega\mu_0 I\delta_{\mathbf{r_0}}$. It can also be the explicit formula $u^i(x,y) = Ae^{ikx}$ if we want to simulate an incident plane wave of amplitude A and of wave vector k; in that case the source $\mathfrak{s}$ vanishes, etc.

$$\Big(\triangle + k_r^2\Big)u^s = [\frac{du}{dn}]\Big|_\Gamma \delta_\Gamma. \tag{13}$$

u^s also satisfies an OWC. Comparing (5) with (13), we conclude that, if

$$i\omega\mu_0 \jmath = [\frac{du}{dn}]\Big|_\Gamma,$$

then u_v^i and u^s satisfy the same partial differential equation with the same boundary condition, and thus $u_v^i = u^s$. Consequently, choosing

$$\jmath = \frac{-1}{i\omega\mu_0}[\frac{du}{dn}]\Big|_\Gamma, \tag{14}$$

we have[10]

$$u_v^i|_\Omega = -u^s|_\Omega = u^i|_\Omega.$$

We note that, given u^i and Γ, the solution **j** of the problem is uniquely determined; thus the "mirage" field u_v^i is also uniquely determined.

If Γ has an arbitrary shape, then u (or more precisely u^s) has to be solved numerically. We then extract the generated current **j** and can do our simulation (obviously, the infinitely conducting metal is now removed). However, if Γ is a circle (say, of radius R and centered at the origin), it is possible to give an explicit expression for **j**.

The electric field generated by the virtual antenna satisfying the equation (5), it has the following Fourier-Bessel expansion:

$$u_v^i(r,\theta) = \begin{cases} \sum_{n\in\mathbb{Z}} \Big(a_n^{in} J_n(k_r r) + b_n^{in} H_n^{(2)}(k_r r)\Big)e^{in\theta}, & r \le R \\ \sum_{n\in\mathbb{Z}} \Big(a_n^{out} J_n(k_r r) + b_n^{out} H_n^{(2)}(k_r r)\Big)e^{in\theta}, & r \ge R \end{cases}$$

Both u_v^i and $\dfrac{du_v^i}{dr}$ do not suffer a jump when crossing Γ. Besides, inside Ω, the field is bounded (by eq.7 and eq.9) so all the b_n^{in} vanish. Outside Ω, u_v^i satisfies an OWC (eq.6) and thus all the a_n^{out} vanish. Moreover, by the requirement (eq.7) that u_v^i restricted to Ω is identical to the incident field, whose development in the Fourier-Bessel functions can be

$$u^i(r,\theta) = \sum_{n\in\mathbb{Z}} a_n J_n(k_r r) e^{in\theta},$$

we have $a_n^{in} = a_n$. Finally, by the continuity condition, we have $b_n^{out} = \dfrac{a_n^{in} J_n(k_r R)}{H_n^{(2)}(k_r R)}$. All the conditions (from eq.5 to eq.9) have been used, so we have this *unique* solution for u_v^i:

[10] $-u^s|_\Omega = u^i|_\Omega$ since u vanishes in Ω.

$$u_v^i(r,\theta) = \begin{cases} \displaystyle\sum_{n\in\mathbb{Z}} a_n J_n(k_r r) e^{in\theta}, & r \leq R \\ \displaystyle\sum_{n\in\mathbb{Z}} \frac{a_n J_n(k_r R)}{H_n^{(2)}(k_r R)} H_n^{(2)}(k_r r) e^{in\theta}, & r \geq R \end{cases}$$

Now, developing $\jmath$ on a Fourier basis,

$$\jmath(r,\theta) = \sum_{n\in\mathbb{Z}} j_n(r) e^{in\theta},$$

and applying the relation (14), we have, after some straightforward computations, the following expression for the current of the virtual antenna:

$$j_n(r) = \frac{a_n k_r}{2i\omega\mu_0} \Big\{ \frac{J_n(k_r R)}{H_n^{(2)}(k_r R)} (H_{n-1}^{(2)} - H_{n+1}^{(2)})(k_r r) - (J_{n-1} - J_{n+1})(k_r r) \Big\}.$$

We recall that, in order to simulate a plane wave of amplitude A, the coefficient a_n is simply Ai^n.

On the figure 6, the current **j** on Γ is presented, as well as the real part of the field $\Re e\{u_v^i\}$.

References

[1] R.W. Boyd. *Non Linear Optics, 2^{nd} edition*. Academic Press, Amsterdam, 2003.

[2] E. Centeno and D. Felbacq. Optical bistability in finite-size nonlinear bidimensional photonic crystals doped by a microcavity. *Physical Review B*, 62(12):7683, 2000.

[3] P. Xie and Z.Q. Zhang. Multifrequency gap solitons in nonlinear photonic crystals. *Physical Review Letters*, 91(21):213904, 2003.

[4] J.P. Bérenger. A perfectly matched layer for the absorption of electromagnetic waves. *Journal of Computational Physics*, 114:185, 1994.

[5] M. Soljacic, M. Ibanescu, S.G. Johnson, Y. Fink, and J.D. Joannopoulos. Optimal bistable switching in nonlinear photonic crystals. *Physical Review E*, 66:55601, 2002.

[6] B. Ulug A. Cicek. Influence of kerr nonlinearity on the band structures of two-dimensional photonic crystals. *ScienceDirect*, 281:3924, 2008.

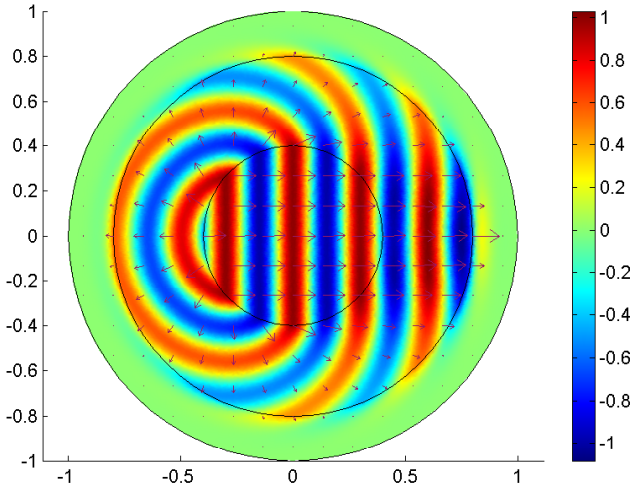

(a) The real part $\Re e\{u_v^i\}$, in V/m, of the field generated by the virtual antenna, and arrows of the line density of the average over a time period of the electromagnetic power $\mathcal{P}_e^{harm}$, in W/m^2.

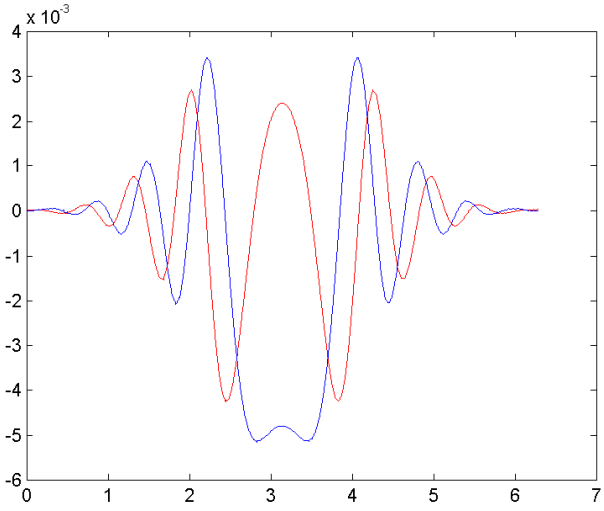

(b) The real (in red) and imaginary (in blue) parts of the current **j**, in A/m, of the virtual antenna, in function of the polar angle.

Figure 6: A plane wave u_v^i is generated in the disk Ω by a current **j** on $\Gamma = \partial\Omega$. Outside of Ω, u_v^i differs from u^i (a plane wave); in particular, u_v^i satisfies an OWC, hence the use of PML (the exterior annulus, in which u_v^i almost vanishes).